sustainability

MDPI

Article

Remote Sensing-Based LULP Change and Its Effect on Ecological Quality in the Context of the Hainan Free Trade Port Plan

Pei Liu [1,2], Tingting Wen [1,2,3], Ruimei Han [4,*], Lin Zhang [1,2] and Yuanping Liu [5]

[1] Hainan Academy of Ocean and Fisheries Sciences, Haikou 572000, China; liupei@hnhky.cn (P.L.)
[2] Yazhou Bay Innovation Institute, Hainan Tropical Ocean University, Sanya 570100, China
[3] School of Surveying and Land Information Engineering, Henan Polytechnic University, Jiaozuo 454003, China
[4] College of Geography and Environmental Sciences, Hainan Normal University, Haikou 571158, China
[5] School of Remote Sensing and Information Engineering, North China Institute of Aerospace Engineering, Langfang 065000, China
* Correspondence: 920275@hainnu.edu.cn

Abstract: The study of Land Use and Landscape Patterns (LULPs) changes and their ecological quality effects in Haikou city under the background of the Hainan Free Trade Port Plan (HFTPP) helps to promote coordinated development between cities and the environment. To date, most research on ecological quality has focused on areas with extremely fragile ecology and/or is related to LULP analysis. There are few studies in the literature focusing on the impact of high-intensity human activities caused by relevant policies on urban LULPs. The purpose of this research was to design a framework that monitors urban ecological security by considering the effect of the developing free trade port. The proposed framework was constructed by integrating multi-temporal Sentinel-2 remote sensing images, night light remote sensing data, digital elevation model (DEM) data, and spectral index features such as the normalized difference vegetation index (NDVI), enhanced vegetation index (EVI), bare soil index (BSI), and normalized intertidal mangrove index (NIMI), as well as analytical approaches such as the land use transfer matrix, land use dynamic degree, land use degree and transfer matrix, land use gravity center measurement, and landscape pattern index. The framework takes advantage of the Google Earth Engine (GEE) cloud platform and was applied to a highly developed Haikou city, the capital of Hainan province. Maps of brightness (SBI), greenness (GVI), and humidity (WET) were created annually from 2016 to 2021, enabling detailed ecological environment quality evaluation and analysis. The advantages of this study are (1) reliable land cover results obtained automatically and quickly; (2) the strong objectivity of the quantitative research on landscape patterns and land use; and (3) deep integration with free trade port policies. Through the research on the ecological quality problems caused by the change in LULP in the study area, the research results show that, from 2016 to 2021, the spatial distribution of land use and landscape pattern in Haikou city had been constantly changing; the area of construction land has decreased, with most of it having been converted into forest land and farmland; the gravity center of the building land has moved to the northwest; the degree of landscape fragmentation has decreased and the heterogeneity of landscape distribution has increased; the free trade port policies have promoted Haikou's economic development and ecological civilization construction; and finally, Haikou's ecological environmental quality has improved significantly.

Keywords: LULP; ecological quality; Google Earth Engine (GEE); Hainan Free Trade Port Plan (HFTPP)

Citation: Liu, P.; Wen, T.; Han, R.; Zhang, L.; Liu, Y. Remote Sensing-Based LULP Change and Its Effect on Ecological Quality in the Context of the Hainan Free Trade Port Plan. *Sustainability* **2024**, *16*, 5311. https://doi.org/10.3390/su16135311

Academic Editor: Zihan Kan

Received: 8 May 2024
Revised: 31 May 2024
Accepted: 19 June 2024
Published: 21 June 2024

1. Introduction

The quality of the ecological environment is an important basis for the sustainable development of human society and an important part of national security [1]. It is also an important guarantee for economic security, political security, and social stability. The

evaluation of the ecological environment quality combined with remote sensing technology and geographic information technology shows the unique characteristics and advantages of interdisciplinary synthesis. Ecological quality evaluation is an important basis for China to promote the construction of ecological civilization and achieve sustainable development, and it is also a hot issue that has been widely considered by academic and political circles in recent years. Haikou, also known as "Coconut City", is the core city of Hainan Free Trade Port. On 13 April 2018, General Secretary Xi Jinping delivered an important speech at the conference to celebrate the 30th anniversary of Hainan's construction of a special economic zone. He supported Hainan in gradually exploring and steadily promoting the construction of a free trade port with Chinese characteristics, and he called for the establishment of a free trade port policy and institutional system step by step [2].

Google Earth Engine (GEE) offers several advantages over other platforms for geospatial analysis and remote sensing. The advantages of GEE can be summarized as follows: (1) GEE hosts a vast collection of satellite imagery and geospatial datasets, including Landsat, Sentinel, MODIS, and more. This extensive archive allows users to access petabytes of data without worrying about storage or data management (https://developers.google.com/earth-engine/datasets (accessed on 3 May 2021)). (2) The Earth Engine is built on Google's cloud infrastructure, which enables scalable and parallelized processing of large-scale geospatial data. Users can analyze terabytes of data in a fraction of the time it would take using traditional computing resources. Earth Engine also provides a wide range of analysis tools and functions for image processing, time series analysis, machine learning, and statistical modeling. These tools are integrated into the platform, making it easier for users to perform complex analyses without switching between different software packages (https://developers.google.com/earth-engine/ (accessed on 3 July 2021)). (3) Earth Engine offers a Code Editor with a JavaScript-based integrated development environment (IDE) that allows users to write, test, and execute code directly in the browser. Additionally, Earth Engine provides APIs for Python and JavaScript, enabling seamless integration with existing workflows and programming languages (https://developers.google.com/earth-engine/playground (accessed on 3 July 2021)). (4) Earth Engine facilitates collaboration and sharing of geospatial data, algorithms, and analysis results through its cloud-based platform. Users can share their code, scripts, and visualizations with others, fostering a collaborative and open-source approach to geospatial research (https://groups.google.com/g/google-earth-engine-users (accessed on 14 November 2021)). (5) In my opinion, the most import advantage is that GEE provides free access to its platform for non-commercial and educational use. This lowers the barrier to entry for researchers, educators, and students who want to explore and analyze geospatial data for various applications, including environmental monitoring, land cover mapping, disaster response, and more (https://earthengine.google.com/terms/ (accessed on 17 November 2021)). These advantages make GEE a powerful platform for geospatial analysis and remote sensing applications, suitable for a wide range of users from researchers and scientists to educators and students [3]. Users can use Java Script and Python programming languages to call upon various images of the platform and develop classification algorithms for remote sensing applications. GEE can support portable and interactive applications, providing great convenience for remote sensing workers [4]. Therefore, in recent years, the GEE cloud platform has been widely used in the field of ecology, based on different scales of the world [5], country [6,7], and region [8,9], involving cities [10], cultivated land [11], watersheds [12,13], and other aspects of ecology environmental studies.

The change in land use and landscape pattern is the result of the interaction between man, nature, and other factors, and it is also an important carrier of economic and social activities [14]. The study of LULP evolution plays a vital role in regional development. At present, research on the change in LULPs is mainly concentrated in ecologically fragile areas [2,15], focusing on long time-series studies [16,17]. However, few researchers have considered the impact of high-intensity human activities and related policies on LULPs in

combination with the conditions of the study area and the general environment of the study area, especially for Haikou City, where the urbanization process has developed rapidly in respect to the free trade port construction in recent years.

In this context, it is of great significance to clarify the impact of the free trade port construction on LULP changes and ecological quality evaluation in Haikou. Therefore, this study took Haikou City as an example, used the GEE cloud platform, selected Sentinel-2 data from 2016 to 2021, and then constructed a feature set to obtain the land cover results of the study area. Then, this study used the land use transfer matrix, land use dynamic degree, land use degree and transfer matrix, land use gravity center measurement, and landscape pattern index to carry out land use and landscape pattern change analysis. Finally, we used indicators such as "brightness (SBI)", "greenness (GVI)", and "humidity (WET)" to evaluate the ecological health of Haikou City and analyze the ecological impact of the free trade port construction on Haikou City. Research outcomes can significantly enhance decision-making for governmental actors striving for more sustainable cities. By utilizing historical satellite imagery and geospatial data from 2016 to 2021 in this research, governmental actors can understand urban growth patterns, identify areas of rapid development, and predict future expansion. In addition, the research overcomes the spatial and temporal limitations of traditional methods and can better reflect the landscape pattern information of surface cover, provide important reference for ecological environmental protection and restoration, and further promote the application and development of remote sensing technology in urban planning and environmental management.

2. Study Area

Haikou City (N 19°31′32″–20°04′52″, E 110°07′22″–110°42′32″) is located in the north of Hainan province, and has a tropical marine monsoon climate. The topography of Haikou is slightly long and heart-shaped, and it is dominated by plains and terraced fields, with rich wetlands and numerous rivers. Haikou has jurisdiction over the districts Xiuying, Longhua, Qiongshan, and Meilan. Haikou is the political, economic, technological, and cultural center of Hainan Province, and it is also the largest transportation hub [18]. The geographical location of the study area is shown in Figure 1.

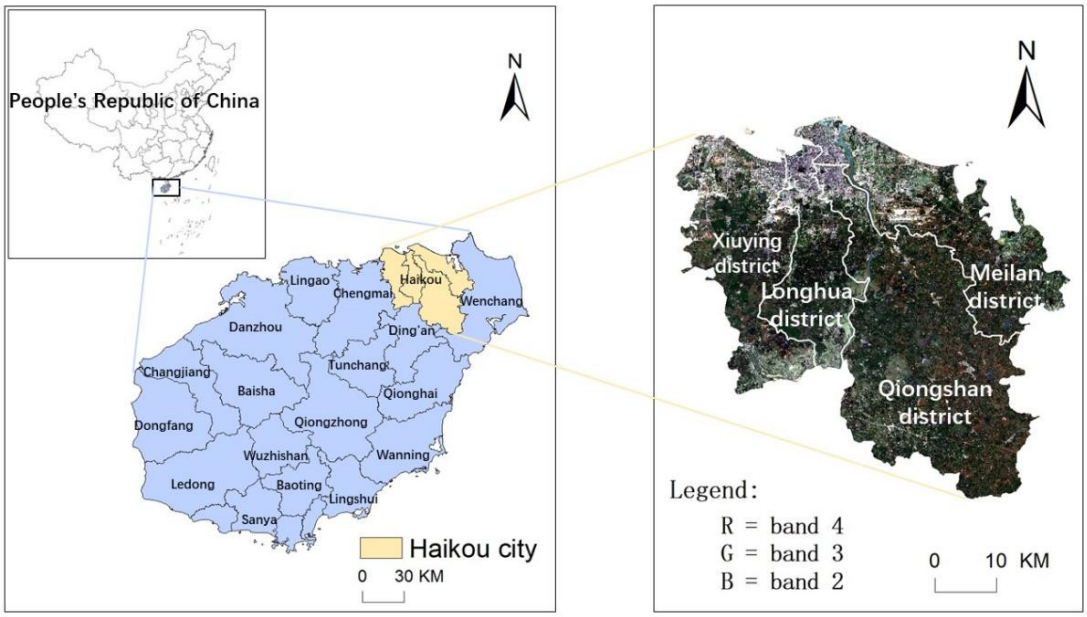

Figure 1. Location of the study area.

3. Data Sources and Preprocessing

3.1. Data Sources

The remote sensing data used in this study mainly include Sentinel-2 satellite data and night light data (VIIRS). These data were acquired through the GEE platform combined with the research area (Haikou City) and time information (2016–2021). The digital elevation model (DEM) data and slope data of Haikou City come from the Resource and Environment Science and Data Center (https://www.resdc.cn/ (accessed on 18 January 2022); the administrative division data come from the National Geomatics Center of China (http://www.ngcc.cn/ngcc/ (accessed on 18 January 2022); and Haikou Statistical Yearbooks come from The People's Government of Hainan Province (https://www.hainan.gov.cn/ (accessed on 27 January 2022).

3.2. Data Preprocessing

The remote sensing data were Sentinel-2 high-resolution multi-spectral images, which are generated by two complementary satellites, with a revisit period of 5 days and an imaging resolution of 10–60 m [19]. The Sentinel-2 images used in this study are products stored in the GEE platform after atmospheric correction and orthorectification. Because the study area has a weather feature with a lot of cloud cover, in order to obtain high-quality image data, we carried out cloud processing. Based on the official method provided by GEE, the study used the QA band to quickly perform cloud remove processing on the Sentinel-2 images. When acquiring Sentinel-2 images of the study area, we limited the percentage of cloud cover (<20%) and chose the median method to synthesize the image data with the minimum cloud cover. The preprocessing of the remote sensing images was completed through steps such as mosaic and cropping. Finally, the basic remote sensing image dataset was obtained.

According to the classification standards in the "Classification of Land Use Status" (GB 21010-2017) [20] and the actual land use/cover classification status of Haikou City, the classification system was divided into eight land use types: grassland, wetland, water, forest land, building land, farmland, bare land, and mangrove. For the high-resolution remote sensing image data in the GEE platform, the collection strategy of "small area continuous collection, global uniform distribution" was used to visually select samples.

4. Methods

4.1. Research Route

Firstly, with the help of the GEE cloud platform, Sentinel-2 images from 2016 to 2021 in the study area were screened out and clouds were removed, feature sets were constructed, and random forest classification was performed; accuracy evaluation and filtering processing were performed on the classification results. Then, with the help of ArcGIS 10.7 software, based on the land cover classification results of Haikou City, land use change analysis was carried out, with methods including transfer matrix, land use dynamic degree, land use degree and transfer matrix, and land use gravity center measurement. Using Fragstats 4.2 software, a series of landscape pattern indices were selected and analyzed. Finally, the greenness, brightness, and humidity indicators were extracted on the GEE cloud platform. Normalized with the help of ENVI 5.3 software, the ecological quality of Haikou City was analyzed. The research results provide a reference for the construction of the Haikou Free Trade Port. Figure 2 shows the overall methodology for this study.

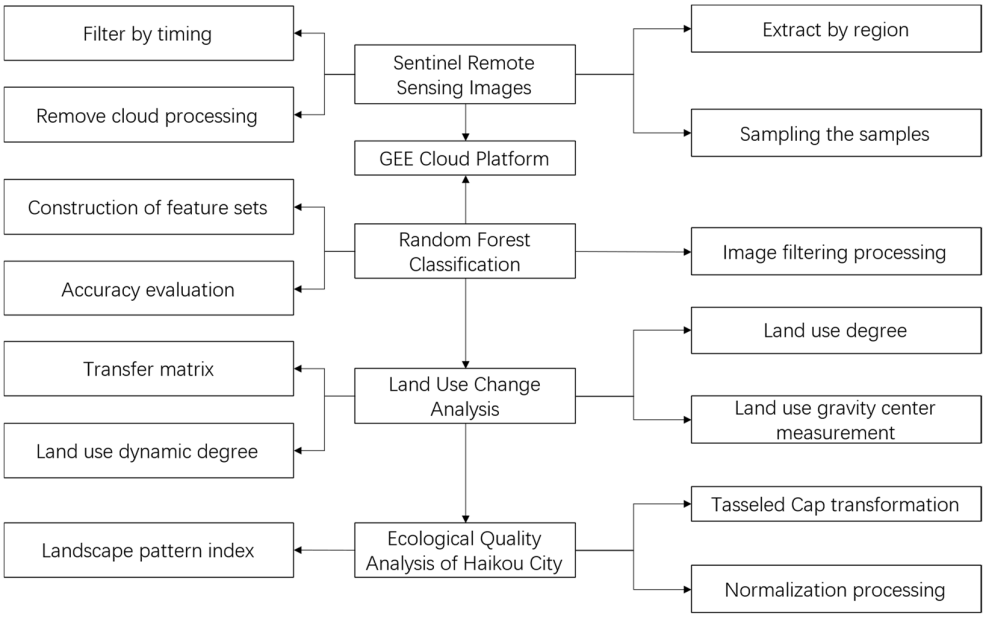

Figure 2. The flow chart of the methodology.

4.2. Land Use Information Extraction

4.2.1. Construction of Feature Set

The selection of feature variables is an important step in remote sensing classification. Using the powerful cloud computing capabilities of the Google Earth Engine platform, for the selected Sentinel-2 remote sensing image dataset, comprehensively considering the characteristics of each band, this study selected the reflectance data of the blue band, green band, red band, near-infrared band, and short-wave infrared band to construct spectral band features, which were used to analyze the spectral difference characteristics of land cover types in Haikou City (Table 1). Using a variety of feature variables and feature variable combinations can effectively improve the accuracy of remote sensing classification. We highlighted ground features by adding spectral index features such as the normalized difference vegetation index (NDVI) [21], enhanced vegetation index (EVI) [22], and bare soil index (BSI) [23]; importantly, we introduced the normalized intertidal mangrove index (NIMI) [24] to extract mangroves. The introduction of night light data can effectively improve the determination of construction land. Topographic features are important features in remote sensing image classification. The elevation information extracted based on DEM data was used as topographic features, which can effectively assist in judging land cover type information at different altitudes.

Table 1. Classification indicators used in the study.

Indicator	Description
Normalized Difference Vegetation Index (NDVI)	$NDVI = \frac{\rho_{NIR}-\rho_{Red}}{\rho_{NIR}+\rho_{Red}}$
Enhanced Vegetation Index (EVI)	$EVI = 2.5 \times \frac{\rho_{NIR}-\rho_{Red}}{\rho_{NIR}+6\times\rho_{Red}-7\times\rho_{Blue}+1}$
Normalized Intertidal Mangrove Index (NMI)	$NIMI = \frac{\left(3\times\rho_{Red}-(\rho_{RedEdge2}+\rho_{RedEdge3}+\rho_{NIR}\right)}{3\times\rho_{Red}+\rho_{RedEdge2}+\rho_{7RedEdge3}+\rho_{NIR}}$
Bare Soil Index (BSI)	$BSI = \frac{[(\rho_{SWIR1}+\rho_{Red})-(\rho_{NIR}+\rho_{Blue})]}{[(\rho_{SWIR1}+\rho_{Red})+(\rho_{NIR}+\rho_{Blue})]}$

Notes: In this formula, ρ_{Blue}, ρ_{Red}, $\rho_{Red\ Edge\ 2}$, $\rho_{Red\ Edge\ 3}$, ρ_{NIR}, and ρ_{SWIR1}, respectively, represent the reflectivity of b2, b4, b6, b7, b8, and b11 in Sentinel-2 image data.

4.2.2. Classification and Filtering

In addition to the data source, the choice in classification algorithm also directly affects the classification results. In recent years, with the development of machine learning

classification algorithms, the random forest algorithm (RF) has high calculation accuracy and less model training time. RF is able to determine the relative importance of variables in the model with low sensitivity to the number and quality of training samples [25]. Therefore, RF is widely used in land cover identification. In this study, the random forest algorithm was used for land use classification in Haikou City; 70% of the sample points were selected as training samples for training the classifier, and 30% of the sample points were used as validation samples for accuracy verification.

Because the topography of the study area breaks up the land use units, the classification results obtained have a "salt and pepper phenomenon", so the classification results need to be post-processed. In this paper, the method of mode filtering was used to remove, merge, and cluster the fragmented image patches after classification. We used the nearest eight-pixel neighborhood as the filter mode, that is, when at least half of the eight pixels are the same, the corresponding pixel value can be changed [23]. This ensures that the spatial structure unit in the classification result is relatively complete.

4.2.3. Accuracy Evaluation

The accuracy of land use classification in Haikou City was verified by the confusion matrix and sample points collected from high-resolution images. The evaluation incorporated several precision metrics, including producer's accuracy (PA), user's accuracy (UA), overall accuracy (OA), and the Kappa coefficient (Kappa). The confusion matrix provides a clear visual representation of the classification results, but it does not readily reveal the accuracy of individual category classifications. With the help of these multiple accuracy metrics, we can gain a comprehensive understanding of the strengths and limitations of our land use classification model in Haikou City. Among these, OA and the Kappa coefficient (Kappa) are particularly noteworthy. Overall accuracy (OA) refers to the ratio of the number of pixels, which is the correctly classified category to the total category, and the Kappa coefficient (Kappa) is an indicator used to measure the consistency of the classification result of the verification sample [26].

$$Overall\ accuracy = \frac{Number\ of\ correct\ plots(value)}{Total\ number\ of\ \ plots(value)} \tag{1}$$

$$Kappa\ coefficient = \frac{\sum_{i=1}^{k} nii - \sum_{i=1}^{k} nii(G_i C_i)}{n^2 - \sum_{i=1}^{k} nii(G_i C_i)} \tag{2}$$

where i is the class number, n is the total number of classified pixels that are being compared to actual data, nii is the number of pixels belonging to the actual data class i which were classified with a class i, C_i is the total number of classified pixels belonging to class i, and G_i is the total number of actual data pixels belonging to class i.

4.3. Land Use Change

4.3.1. Land Use Transition Matrix

The land use transfer matrix can quantitatively reflect the structure and transfer changes in land types in different periods. Its mathematical expression is shown in (3). Based on ArcGIS 10.7 software, using the Dissolve Tool and the Intersect Tool, combined with Excel 2016 software, a total of six periods of land use transfer data from 2016 to 2021 were generated. These data were used to analyze the characteristics of land use quantity and direction in Haikou City.

$$S_{ij} = \begin{bmatrix} S_{11} & S_{12} & \cdots & S_{1n} \\ S_{21} & S_{22} & \cdots & S_{2n} \\ \cdots & \cdots & \cdots & \cdots \\ S_{n1} & S_{n2} & \cdots & S_{nn} \end{bmatrix} \tag{3}$$

In this formula, S_{ij} is the area of land type i converted into land type j, and n is the number of land use types.

4.3.2. Land Use Dynamic Degree

(1) The Single Land Use Dynamic Degree.

The dynamic degree of a single land use type expresses the quantity changes in a certain land use type within a certain time range in a certain research area. In this paper, it is expressed as the annual change rate [27], and its expression formula is (4).

$$K = \frac{U_b - U_a}{U_a} \times \frac{1}{T} \times 100\% \quad (4)$$

In the formula, K is the annual change rate of a certain type of land use during the study period; U_a and U_b are the areas of a certain type of land use at the beginning and end of the study period, respectively; and T is the length of the study period.

(2) The Integrated Land Use Dynamic Degree

The integrated dynamic index of land use is the transfer rate among land categories during the research period. The calculation formula of the integrated land use dynamic degree in Haikou [28] is shown in (5).

$$k_{total} = \left(\frac{\sum_{i=1}^{n} |U_{bi} - U_{ai}|}{2\sum_{i=1}^{n} U_{ai}} \right) \times \frac{1}{T} \times 100\% \quad (5)$$

In this equation, U_{bi} and U_{ai} are the areas of a certain land use category at the end and beginning moment of the research, respectively, T is the duration of the study, and n is the quantity of land use categories and is equal to eight in this study. When T is year(s), k_{total} is the annual integrated change rate of area change in all land use categories.

4.3.3. Land Use Degree

The land use degree reflects the breadth and depth of land use. It also reflects the comprehensive effects of human activities and the natural environment on land use [29]. According to the comprehensive analysis method of land use degree proposed by Zhuang Dafang et al. [30], this paper divides the land use degree into four grades according to the land natural complex in a state of natural balance. The assigned grading indices are shown in Table 2.

Table 2. Classification values of land use degree classification index.

Land Use Classification	Land Use Type	Land Use Degree Classification Index: A_i
Uncultivated land level	Bare land	1
Grass and water with ground level	Forest land, grassland, water, mangrove, wetland	2
Agriculture land level	Farmland	3
Urban Community land level	Building land	4

(1) Land Use Degree Index

The land use degree index model [31] is (6):

$$L_j = 100 \times \sum_{i=1}^{n} A_i \times C_i \quad (6)$$

In the formula, L_j is the index of land use degree; A_i is the grading index of the i-level land use degree; C_i is the area percentage of the i-level land use degree; and n is the grade of the land use degree. The change interval of the land use degree index is [100, 400]; the higher the land use degree, the larger the index.

(2) Rate of land use degree

The rate of the land use degree model [32] is formula (7):

$$R = \frac{\sum_{i=1}^{n} A_i \times C_{ib} - \sum_{i=1}^{n} A_i \times C_{ia}}{\sum_{i=1}^{n} A_i \times C_{ia}} \times 100\% \quad (7)$$

In the formula, R is the change rate of the land use degree; A_i is the grading index of the i-level land use degree; and C_{ib} and C_{ia} are the percentages of the area occupied by the i-level land use degree at time b and time a. If R is positive, the land use in this area is in the development period, and if R is negative, it means that it is in the adjustment period or the decline period.

4.3.4. Land Use Gravity Center Measurement

Land use gravity center, that is, the geometric balance point of a land use type, is an important indicator to measure the overall distribution of a certain land use type in a region [33]. By comparing the gravity center distribution of land use types at the beginning and end of the research period, we can obtain the characteristics of land use change and distribution in a certain period of time. This index mainly reflects the concentrated distribution of land use types in space. The calculation formulas are shown in Formula (8) and Formula (9):

$$X_t = \frac{\sum_{i=1}^{n} X_i M_{it}}{\sum_{i=1}^{n} M_{it}} \quad (8)$$

$$Y_t = \sum_{i=1}^{n} Y_i M_{it} / \sum_{i=1}^{n} M_{it} \quad (9)$$

In the formula, X_t and Y_t are the gravity center coordinates of a certain land use type in year t; n is the number of patches; C_n is the area of a certain land use type; X_i and Y_i are the barycentric longitude and latitude of the i-th patch, respectively; and M_{it} is the area of the i-th patch in year t.

4.4. Ecological Quality Analysis

4.4.1. Landscape Pattern Index

The landscape pattern index is a quantitative index that reflects the spatial layout and structural composition characteristics of landscape elements. It can highly reflect the landscape pattern information [34]. The landscape pattern index is divided into three levels, which are patch level index, class level index, and landscape level index [35]. Referring to the previous research, at the patch-type level, this paper selected the number of patches index (NP), the mean patch area index (AREA_MN), the largest patch index (LPI), and the landscape shape index (LSI) to analyze the changes in landscape pattern. At the landscape level, indices such as the mean patch area index (AREA_MN), the largest patch index (LPI), the landscape shape index (LSI), the patch density index (PD), Shannon's diversity index (SHDI), and Shannon's evenness index (SHEI) were selected to analyze the landscape pattern changes. Fragstats 4.2 software provides a large number of spatial metrics, and a specific subset of them were specifically selected for this study; they are described in Table 3 [36,37].

Table 3. Spatial metrics selected in this study.

Abbreviation	Metrics	Description
NP	Number of patches	Total number of patches in the landscape.
PD	Patch density	The number of patches per 100 ha.
AREA_MN	Mean patch area	This indicates the degree of landscape fragmentation. The smaller the value, the more fragmented the landscape is.
LPI	Largest patch index	$0 < \text{LPI} \leq 100$. LPI approaches 0 when the largest patch in the landscape is increasingly small. LPI = 100 when the entire landscape consists of a single patch; that is, when the largest patch contains 100% of the landscape. Its change can reflect the change in the intensity of human disturbance activities.

Table 3. *Cont.*

Abbreviation	Metrics	Description
LSI	Landscape shape index	The total length of edge in the landscape divided by the minimum total length of edge possible.
SHDI	Shannon's diversity index	SHDI ≥ 0. The increase in SHDI value indicates an increase in landscape patch types or a more balanced distribution trend in the landscape.
SHEI	Shannon's evenness index	$0 \leq$ SHEI ≤ 1. This provides information on area richness and composition. A measurement of patch diversity, which is determined by the distribution of different types of patches in landscape.

4.4.2. Ecological Quality Assessment

This study conducted rapid monitoring and evaluation of the regional ecological environment based on remote sensing information. On the basis of the obtained tasseled cap transformation results, the research used the GEE platform to synthesize the humidity, brightness, and greenness to construct and describe the spatial distribution of the ecological environment quality.

(1) Tasseled Cap Transformation

Tasseled cap transformation is an orthogonal transformation of images based on the distribution structure of soil, vegetation, and other information in multidimensional spectral space [38]. The transformed main components are "Soil Brightness Index (SBI)", "Vegetation Greenness Index (GVI)", and "Wetness (WET)", which, respectively, reflect information such as soil rocks, vegetation, and moisture in soil and vegetation. The information represented by these components can be applied to ecological environment monitoring. The tasseled cap transformation depends on the band settings and characteristics of the sensor itself, and the transformation coefficients of different sensors are not universal. In this study, referring to previous research results [39], the corresponding transformation coefficients were set to calculate the SBI, GVI, WET, and other components of Sentinel-2 data. The transformation matrix formula is shown in (10).

$$\begin{bmatrix} SBI \\ GVI \\ WET \end{bmatrix} = \begin{bmatrix} 0.3037 & -0.2848 & 0.1509 \\ 0.2793 & -0.2435 & 0.1973 \\ 0.4743 & -0.5436 & 0.3279 \\ 0.5585 & 0.7243 & 0.3406 \\ 0.5082 & 0.0840 & -0.7112 \\ 0.1863 & -0.1800 & -0.4572 \end{bmatrix}^T \begin{bmatrix} B_2 \\ B_3 \\ B_4 \\ B_8 \\ B_{11} \\ B_{12} \end{bmatrix} \quad (10)$$

In the formula, B_2, B_3, B_4, B_8, B_{11}, and B_{12} are the band values corresponding to Sentinel-2.

(2) Normalization Processing

According to the correlation between each index value and the ecological environment, the corresponding method was used to normalize the initial calculation results [40]. For positive correlation indicators, the normalization formula is (11). For negative correlation indicators, the normalization formula is (12).

$$y_i = \frac{x_i - x_{min}}{x_{max} - x_{min}} \quad (11)$$

$$y_i = 1 - \frac{x_i - x_{min}}{x_{max} - x_{min}} \quad (12)$$

In the formula, y_i is the index score after normalization, and x_i, x_{min}, and x_{max} are the initial value, minimum value, and maximum value of the indicator, respectively.

5. Results and Analysis

5.1. The Spatiotemporal Changes in Land Use in Haikou City

The spatiotemporal distribution of land use in Haikou City was evaluated utilizing the GEE platform and the random forest classification algorithm, followed by spatial connectivity processing with the filter mode. The resulting map, after the removal of small patches, is presented in Figure 3. The accuracy evaluation of the land use data of Haikou City in each period was carried out, and the results are shown in Table 4. We found that the overall accuracy (OA) and the Kappa coefficient of land use in each period were greater than 0.85, meeting the relevant accuracy requirements. By showing the classified statistics of the data on land use types in Haikou City from 2016 to 2021 (see Table 5), this table can succinctly express the area changes in different years. The results show that there are obvious regional differences in the distribution of land use types in Haikou City. The user accuracy (UA) of building land from 2016 to 2021 was 0.92, 1, 1, 0.85, 1, 0.77, and 0.97, respectively, while the production accuracy (PA) was 0.79, 0.95, 0.94, 1, 1, and 1, respectively, all maintained at a high level. These results show that our classification algorithm can accurately distinguish building land from other land types in most cases. On the whole, forest land, building land, and farmland are the main types, among which forest land occupies the largest area. From the perspective of spatial distribution, forest land is widely distributed, mainly in the central, western, and southeastern regions of Haikou, except for buildings; mangroves are mainly distributed in the northeastern coastal area; and building land is mainly distributed in the northern part of Haikou. The water network of rivers and lakes in Haikou City is densely distributed, and the water area is mainly located in the Nandu River flow area, which runs from south to north. The proportion of bare land and wetland is relatively small, indicating that Haikou has a high degree of land development and utilization, and the reserve land resources are not sufficient.

Table 4. Accuracy evaluation of classification results.

Years	Projects	Grassland	Wetland	Water	Forest Land	Building Land	Bare Land	Farmland	Mangrove	OA	KAPPA
2016	UA	0.78	0.67	1	0.90	0.92	0.93	0.83	0.83	0.89	0.86
	PA	1	0.67	0.94	0.95	0.79	0.82	0.88	1		
2017	UA	1	1	1	1	1	0.92	0.92	1	0.98	0.98
	PA	1	1	1	1	0.95	0.95	1	1		
2018	UA	1	1	0.96	0.87	1	0.81	0.90	1	0.94	0.93
	PA	0.95	0.56	1	1	0.94	0.93	0.95	1		
2019	UA	1	0.67	1	1	0.85	1	0.93	1	0.95	0.95
	PA	0.88	1	1	1	0.94	0.92	1	1		
2020	UA	1	1	1	0.76	0.77	1	0.94	1	0.91	0.89
	PA	0.91	1	1	0.84	1	0.88	0.75	1		
2021	UA	0.95	1	1	0.94	0.97	1	0.84	1	0.95	0.943
	PA	0.95	0.80	1	0.89	1	0.90	0.94	1		

Table 5. The land use transfer matrix of Haikou from 2016 to 2021 (km^2).

		2021									
		Grassland	Wetland	Water	Forest Land	Building Land	Bare Land	Farmland	Mangrove	Initial Total	Gross Loss
2016	Grassland	26.145	0.727	0.160	52.755	43.885	0.199	39.614	0.069	163.555	137.410
	Wetland	0.325	3.373	3.353	3.650	1.262	0.078	5.325	0.013	17.378	17.054
	Water	0.368	8.912	59.973	1.019	24.960	0.466	9.640	0.076	105.414	105.046
	Forest Land	12.523	1.803	0.486	738.938	41.958	2.804	188.813	0.850	988.175	975.652
	Building	42.866	3.326	3.870	158.066	446.923	2.792	202.713	0.322	860.877	818.011
	Bare Land	0.188	0.075	0.348	0.239	15.536	3.347	0.772	0.001	20.506	20.318
	Farmland	7.842	5.552	1.674	106.685	31.659	2.060	179.616	0.250	335.339	327.497
	Mangrove	1.835	0.266	0.333	9.155	11.665	0.017	9.138	1.515	33.923	32.089
	Initial Total	92.092	24.033	70.198	1070.508	617.849	11.761	635.632	3.096	2525.168	-
	Gross Gain	65.947	23.306	70.038	1017.753	573.963	11.562	596.017	3.026	-	-

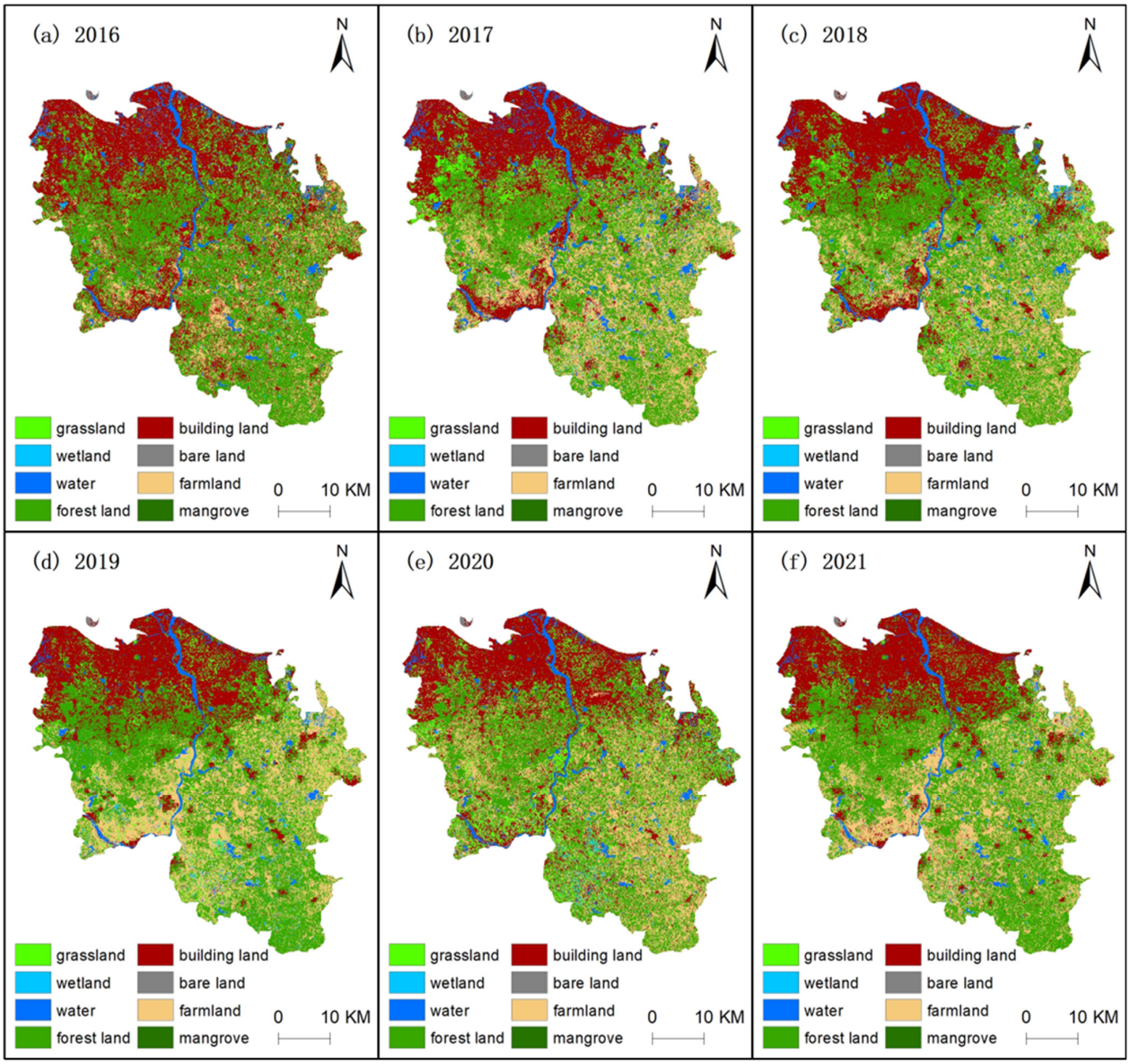

Figure 3. Classified maps of Haikou: (**a**) in 2016; (**b**) in 2017; (**c**) in 2018; (**d**) in 2019; (**e**) in 2020; and (**f**) in 2021.

5.1.1. Analysis of Land Use Transfer Matrix

We used the ARCGIS software to export the attribute table, and then obtained the land use transfer matrix table in Excel. The table clearly shows the characteristics and rules of the internal conversion among land use types in Haikou City. In the conversion of land use types, grassland is the most converted, and it is mainly converted into forest land; the converted grassland area amounts to 52.755 km^2. The second most converted is building land, whose converted area is 43.885 km^2. Wetland is mainly converted into farmland; water, bare land, and mangroves are mainly converted into building land; building land is mainly converted into farmland and forest land; and farmland is mainly converted into forest land. The land use transfer matrix from 2016 to 2021 is shown in Table 5.

5.1.2. Analysis of Land Use Dynamic Degree

It can be seen from the land use dynamic degree results (Table 6) that the integrated land use dynamic degree in the five periods shows a trend of decreasing first and then increasing. From 2016 to 2017, the integrated land use dynamic degree was the highest,

with a value of 13.789%, mainly due to the increase in farmland. At this time, the single land use dynamic degree was 90.482%. The integrated land use dynamic degree during 2018–2019 was 5.727%, which was the lowest value among the five periods. This change was mainly caused by the increase in farmland area. During 2017–2018, the area of farmland decreased the most, and its single land use dynamic degree was −18.215%. During the period of 2019–2020, the mangroves changed greatly, and their single land use dynamic degree was 290.424%. The type of surface cover with the largest increase in area during 2020–2021 was forest land, and its single dynamic degree was 27.633%.

Table 6. The land use dynamic degree and change rate of Haikou from 2016 to 2021.

Single Land Use Dynamic Degree (%)	2016–2017	2017–2018	2018–2019	2019–2020	2020–2021
Grassland	−5.094	15.409	−8.242	38.641	−59.590
Wetland	10.864	152.066	−31.757	12.951	−35.797
Water	34.947	−41.246	8.284	−6.620	−16.938
Forest Land	−13.293	13.582	0.775	−14.478	27.633
Building Land	−20.709	3.096	−15.998	17.896	−11.348
Bare Land	29.528	−63.541	77.788	−25.632	−8.146
Farmland	90.482	−18.215	23.472	−4.646	3.344
Mangrove	−89.105	31.818	−38.054	290.424	−73.725
Integrated Land Use Dynamic Degree (%)	13.789	7.600	5.727	7.222	9.993
Land Use Degree Change Rate (%)	−0.835	−0.813	−1.580	2.712	−1.937

5.1.3. Analysis of Land Use Degree

The research divided the land use types into four grades, and Figure 4 shows a map of the land use degree changes in the six phases in this area. From the analysis of the figure, we can conclude that the degree of land use presents a trend of first decreasing, then increasing, and then decreasing. The change interval of the land use degree index is [100, 400]; the higher the land use degree, the greater the index value. It can be seen from the land use degree change map of Haikou City that the degree dropped from 280.652 in 2016 to 271.682 in 2019, then increased to 279.050 in 2020, and then slightly decreased to 273.646 in 2021. On the whole, the degree of land use showed a decline, indicating that land use has been in a stage of constant adjustment during this period. Haikou is gradually figuring out its own development mode, which requires us to pay attention to the construction of ecological civilization, constantly adjust the way the land is used, and finally, improve the efficiency of the land use. The decrease in the land use degree index also indirectly proves that Haikou's ecological environment protection has achieved certain results.

The calculated results of the land use degree change rate in Haikou City in the five stages are shown in Table 6. From this table, we can see that the land use degree change rate in the five periods has positive and negative values. The land use degree change rate in 2016–2020 and 2020–2021 are both negative, and in these two periods, Haikou belonged to the adjustment stage, indicating that the degree of land use by human activities was low, the land load in these periods was small, and the natural state was good. From 2019 to 2020, the land use degree change rate in Haikou City was 2.712%, which is a positive value, indicating that Haikou City was in the development period during this time, meaning that the degree of land use by human activities was increasing. At this stage, the output value of land was constantly changing, and Haikou was gradually entering into a stage of adjustment and development.

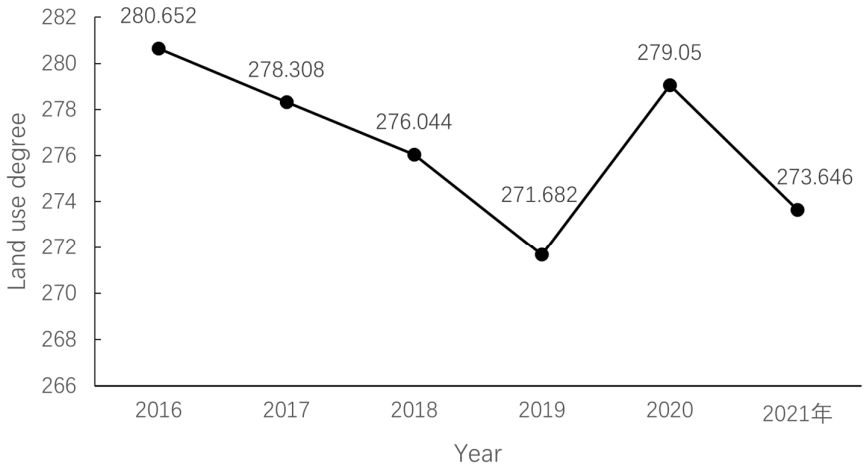

Figure 4. Line chart of land use degree changes in Haikou.

5.1.4. Analysis of the Gravity Center Shift of Building Land in Haikou

In ArcGIS, the average center of building land distribution was calculated for the layers of the past years, so as to represent the gravity center of the building land area. This made it easier to further understand the spatial distribution of the building land. It can be seen from the gravity center transfer map (Figure 5) that the gravity center of the building land during the research period was entirely in Qiongshan District. The gravity center of the building land moved from the southeast to the northwest of Haikou as a whole. During the three stages of 2016–2017, 2018–2019, and 2020–2021, the gravity center of building land moved to the northwest, while the gravity center of building land during 2017–2018 and 2019–2020 moved to the southeast.

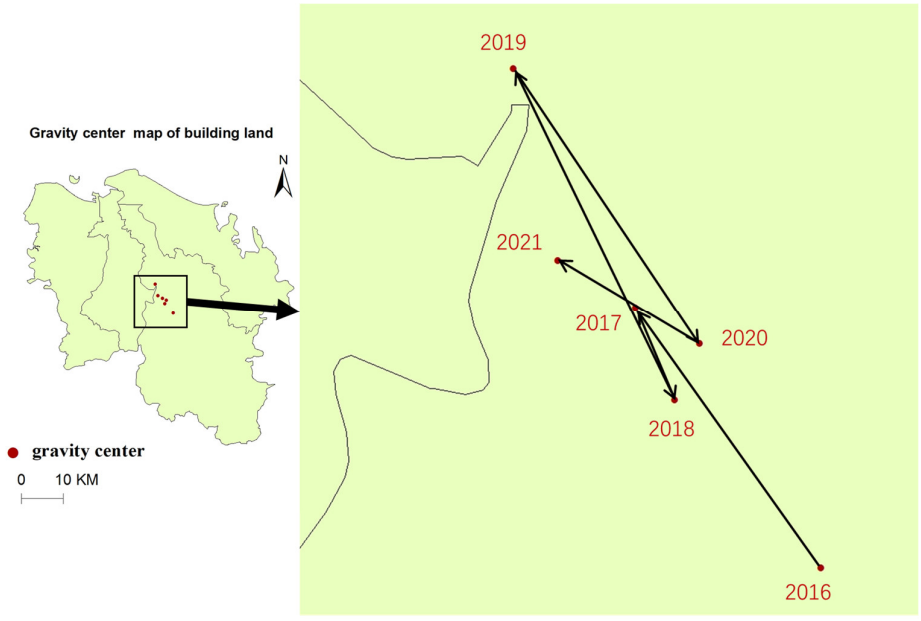

Figure 5. The gravity center shift of building land in Haikou City.

5.2. Analysis of Landscape Pattern Changes

5.2.1. Analysis of Landscape Pattern Changes at Landscape Level

The results of the landscape pattern index of Haikou City at the landscape level from 2016 to 2021 are shown in Figure 6. It can be seen from the figure that the landscape pattern of Haikou City from 2016 to 2021 generally shows the characteristics of gradually increasing landscape fragmentation, simplifying the shape of the landscape, and increasing landscape

heterogeneity. From 2016 to 2021, the mean patch area and patch density in Haikou City have alternating changes of increase and decrease. The mean patch area reached its maximum in 2019, with an area of 0.93 hm^2. Overall, the mean patch area increased from 0.612 hm^2 in 2016 to 0.698 hm^2 in 2021. The patch density reached 1556.857 pieces/100 hm^2 in 2020. These show that under the influence of the external environment, Haikou's landscape distribution is becoming increasingly fragmented, and the degree of interlacing is deepening. As we can see from Figure 6c, the landscape shape index dropped from 380.431 in 2016 to 315.534. The overall decline in the landscape shape index indicates that the distribution of various types of patches in Haikou is becoming more and more compact, and the shape of the patches is more regular and simplified. The constant changes in the largest patch index, Shannon's diversity index, and Shannon's evenness index indicate that the landscape planning of Haikou City has been constantly adjusted. The largest patch index decreased from 19.711 in 2016 to 19.106 in 2021, while Shannon's diversity index and Shannon's evenness index decreased overall. This indicates that the proportional gap between various types of landscapes was slightly increasing. Some dominant landscapes are more prominent, the diversity and balance of the landscapes are relatively reduced, and the heterogeneity of landscape distribution is increasing.

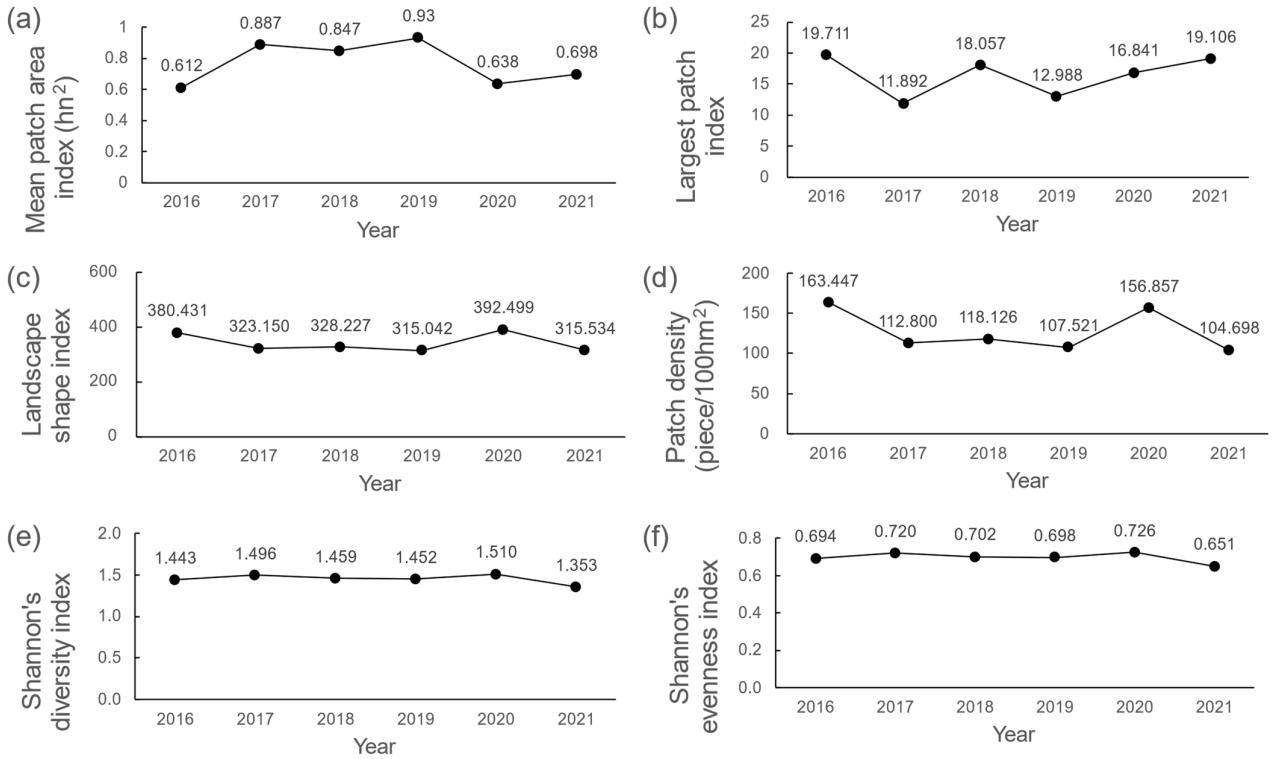

Figure 6. Changes in landscape pattern index at the landscape level: (**a**) mean patch area index; (**b**) largest patch index; (**c**) landscape shape index; (**d**) patch density; (**e**) Shannon's diversity index; and (**f**) Shannon's evenness index.

5.2.2. Analysis of Landscape Pattern Changes at Class Level

From 2016 to 2021, the landscape pattern of Haikou at a class level underwent great changes, and the results are shown in Figure 7. From Figure 7a, it can be seen that the number of patches of grassland, bare land, building land, mangroves, and water showed a decreasing trend from 2016 to 2021, while the number of patches of wetland, forest land, and farmland showed an increasing trend. Among them, the number of forest land patches decreased sharply during 2019–2020; the number of wetland patches continued to increase from 2016 to 2018, which may be due to the issuance of the "Notice of Haikou City on the Implementation of the Key Points for the Construction of Ecological Civilization in

Hainan Province in 2016". We must continue to strengthen the construction of ecological civilization, carry out the construction of ecological restoration in a planned way, and vigorously protect wetland resources. It can be seen from Figure 7b that the mean patch area of wetland, bare land, mangrove, and grassland during the study period is relatively small, indicating that their patches were relatively fragmented. In 2017, the mean patch area of wetland was the smallest, which was 0.0913 hm^2. The mean patch area index of building land, water, and farmland showed alternating changes of increasing and decreasing, but generally increased slightly. Forest land fragmentation decreased during 2020–2021. This indicates that the degree of fragmentation of these three landscape types decreased. From the largest patch index in Figure 7c, it can be seen that the building landscape has increased rapidly overall, indicating that its dominant position has continuously improved. The largest patch index of forest land fluctuated greatly, with a maximum of 19.7107 in 2016 and a minimum of 3.4054 in 2020. The reason may be the rapid economic development and the acceleration of urbanization in recent years. It can be seen from Figure 7d that the landscape shape of the bare land is the most complex, and the landscape shape of the mangrove is relatively simple. Except for bare land, the landscape shape index of all landscape types increased during 2019–2020, indicating that the landscape shape became more complex during this period.

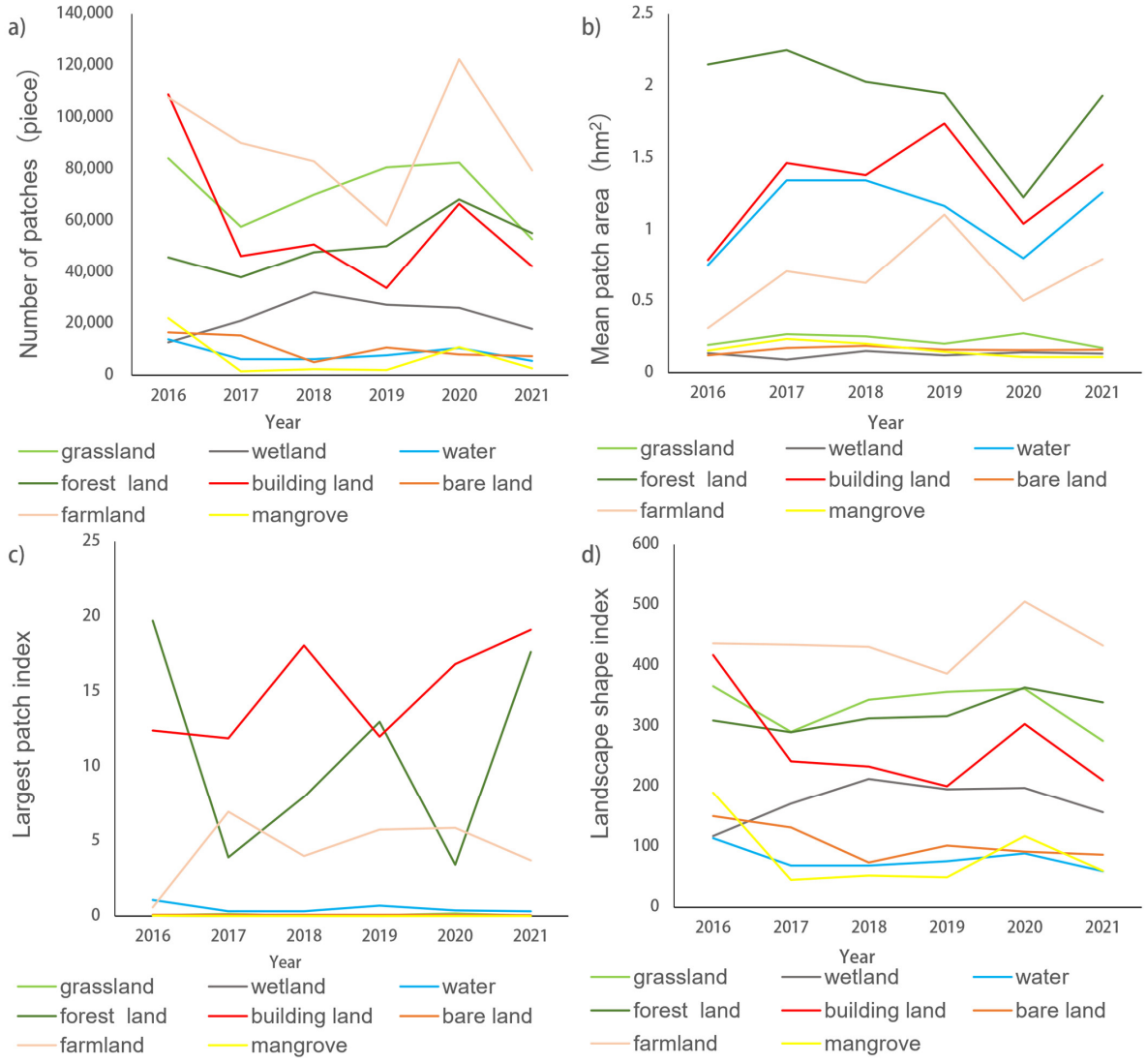

Figure 7. Changes in landscape pattern index at the class level: (**a**) number of patches; (**b**) mean patch area; (**c**) largest patch index; and (**d**) landscape shape index.

5.3. Analysis of Landscape Pattern Changes

The normalized results of the three indicators (brightness, greenness, and humidity) of Haikou City from 2016 to 2021 are shown in Figure 8. Combined with the statistical results (Table 7) of the three indicators (SBI, GVI, and WET) from 2016 to 2021, we can determine that the mean brightness of Haikou in 2016 was 0.5997. From then, the standard deviation of brightness value first decreased and then increased until it reached 0.5848 in 2021. Comparing the brightness distribution maps from 2016 to 2021, it can be clearly seen that the brightness values in the northeast and northwest corners of Haikou City decreased significantly. As for the greenness distribution maps, it is easy to observe that the southern part of Haikou City has a higher greenness value. One reason for this is that forest land and farmland are mostly distributed here. Another reason is that the building land is gathered in the northern part of Haikou, and more human activities have resulted in the destruction of the ecological environment. The mean value of greenness first decreased and then increased, and the overall greenness value increased, showing that the green area of Haikou City has generally increased and the ecological environment has gradually improved. The standard deviation of humidity in Haikou City in 2016 was 0.0386. The mean value of WET first decreased and then increased during 2016–2021, with small-scale changes showing a downward trend overall. From the spatial distribution maps of humidity, it can be seen that the areas with high humidity in Haikou City are distributed along the northern coast of Haikou. The changes in humidity are related to the population density and regional economic development. The decrease in humidity value may be caused by the increase in population and the acceleration of regional economic development. It can be clearly observed from the ecological environment quality distribution maps of Haikou City in 2016 and 2021 (Figure 9) that the ecology of Haikou City in 2021 improved significantly compared to 2016, indicating that the overall quality of the ecological environment improved. The areas with better ecology are mainly distributed in the central and southern vegetation coverage areas, while the ecology of rivers, urban centers, and coastal areas is poor, which is closely related to the scope of human activities.

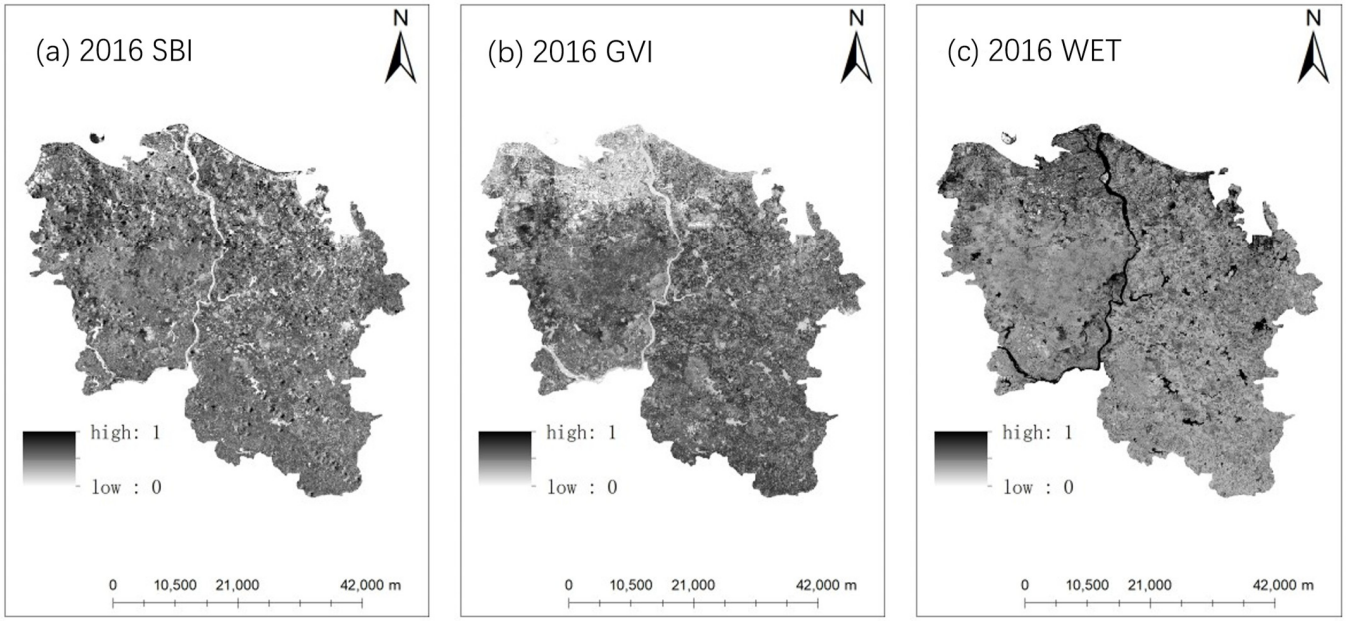

Figure 8. *Cont.*

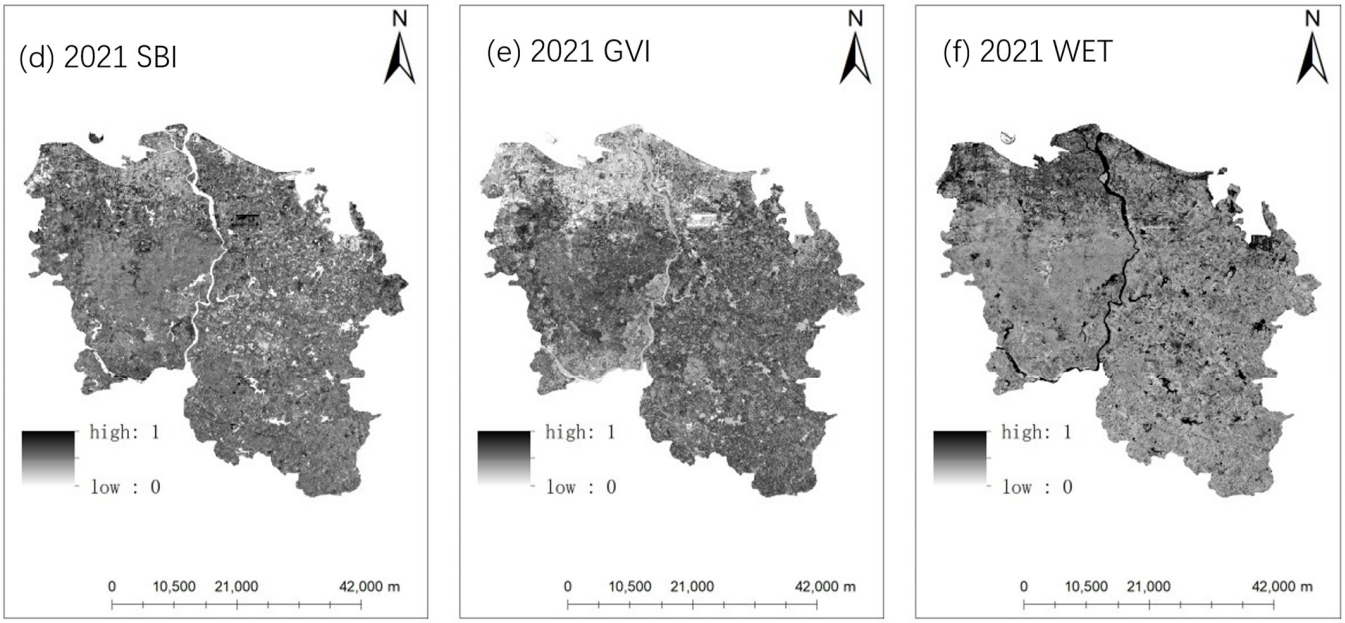

Figure 8. The SBI, GVI, and WET maps of Haikou in 2016 and 2021.

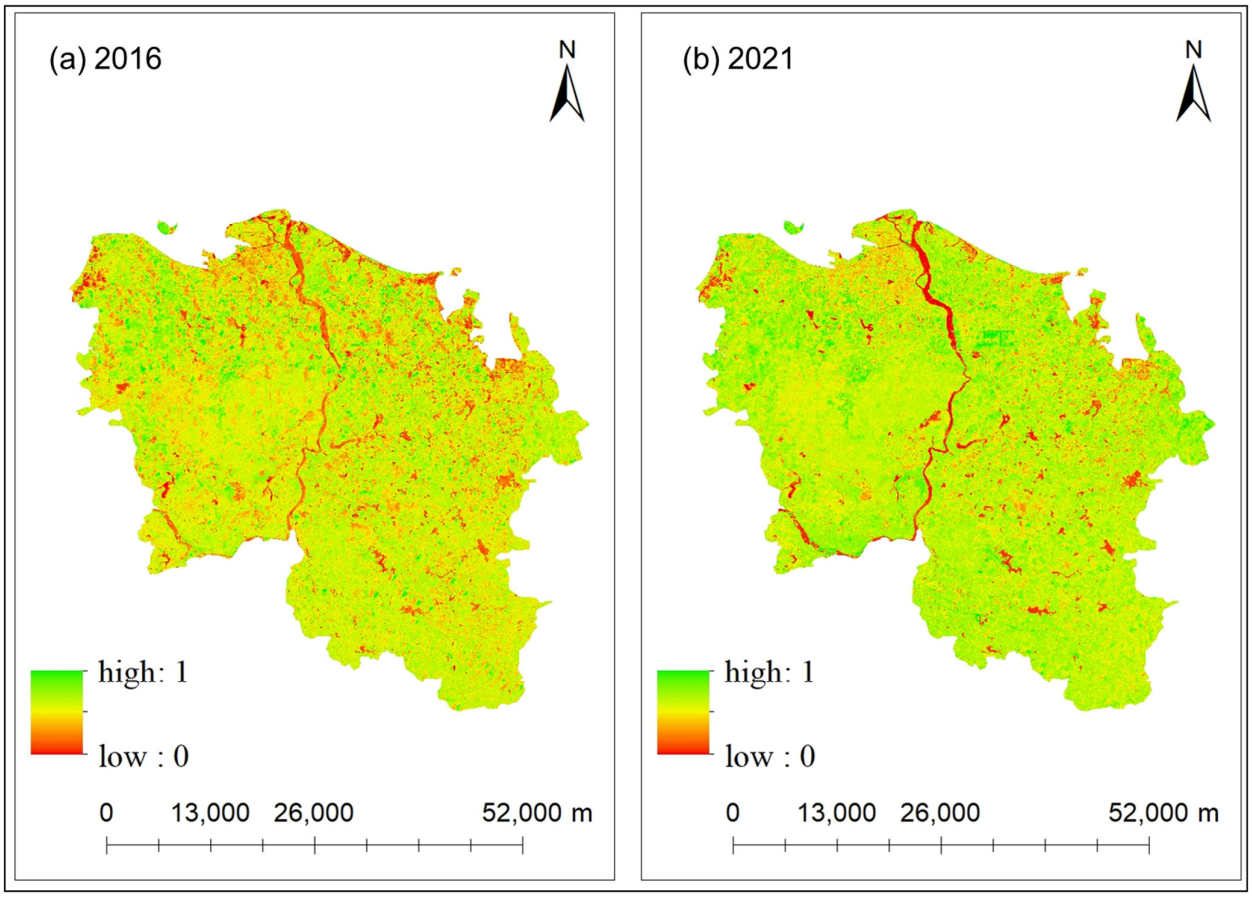

Figure 9. Distribution maps of Haikou's ecological environment quality in 2016 and 2021: (**a**) in 2016 and (**b**) in 2021.

Table 7. The results of SBI, GVI, and WET of Haikou from 2016 to 2021.

Year	SBI		GVI		WET	
	Mean	Standard Deviation	Mean	Standard Deviation	Mean	Standard Deviation
2016	0.5997	0.1262	0.0817	0.0931	−0.0127	0.0386
2017	0.5508	0.1120	0.0662	0.0791	−0.0084	0.0332
2018	0.5558	0.1027	0.0510	0.0738	−0.0093	0.0327
2019	0.5983	0.1334	0.0727	0.0911	−0.0580	0.0107
2020	0.6165	0.1324	0.0714	0.0945	−0.0619	0.0411
2021	0.5848	0.1404	0.0902	0.0974	−0.0648	0.0394

6. Conclusions

This paper analyzed the land use classification results of Haikou City based on the GEE platform. In the context of the Hainan Free Trade Port policy, Haikou City has undergone tremendous changes in LULP. The results of this study will play an important role in maintaining the sustainable development of Haikou City in order to provide a basis and guidance for the ecological restoration and free trade port construction of Haikou City.

The main conclusions are as follows:

(1) This paper uses methods such as the land use transfer matrix, land use degree, land use dynamic degree, and land use gravity center measurement to quantitatively analyze the land use changes in Haikou during the period from 2016 to 2021. The building land in Haikou City is mainly distributed in the northern coastal area; the central and southern parts of Haikou are rich in forest land and farmland; and the mangroves are mostly distributed in the northeastern coastal area of Haikou. In the past six years, the area of building land in Haikou City has decreased overall, while the area of forest land, farmland, and wetland has increased. In recent years, Hainan Province's idle land disposal policy has been continuously improved, and the province's farmland, permanent basic farmland, forest land, etc., are being approved and incorporated into the national land space planning, which is conducive to promoting land use changes in Haikou City. The overall shift in the building's gravity center to the northwest of Haikou is also inseparable from the rapid economic development.

(2) Regarding the landscape, in the research stage, the degree of landscape fragmentation in Haikou City has decreased, the landscape shape has become increasingly simple, and the heterogeneity of landscape distribution has increased. During the development of the free trade port plan, in terms of the operation mode, Haikou has explored a more flexible policy system in terms of domestic and foreign trade and investment. Based on the economic development of various industries such as tourism, the building land has increased rapidly, and its dominant position has been continuously improved, making Haikou's island-based economy and society develop with high quality. While developing the economy, people are advocating for green development and insisting on thick planting and openness, so that the gap between various landscape types is gradually reduced, which gradually reduces the gap between various landscape types and reduces the degree of landscape fragmentation.

(3) After comparing the normalized ecological quality maps of the two periods, 2016 and 2021, it is easy to conclude that the ecological quality of Haikou City improved significantly during the study period. Since the construction of the free trade port requires the protection of the ecological environment, the six iconic projects such as the construction of national parks and the construction of clean energy islands have also achieved certain results. Most of the areas where the ecological environment has improved are forest parks, wetland parks, woodlands, and grasslands; most of the areas with poor ecological environment quality are vegetation-free areas and new construction areas. This shows that the ecological construction promoted by the

Hainan Free Trade Port has a positive effect on improving the environmental quality of Haikou City.

Author Contributions: Conceptualization, P.L. and T.W.; methodology, P.L. and R.H.; validation, P.L., R.H., and L.Z.; writing—original draft preparation, P.L.; writing—review and editing, P.L., T.W. and R.H.; supervision, P.L.; project administration, P.L.; funding acquisition, Y.L. All authors have read and agreed to the published version of the manuscript.

Funding: This research was funded by the Hainan Provincial Natural Science Foundation of China (423MS120), the Open Project Program of Yazhou Bay Innovation Institute of Hainan Tropical Ocean University (2022CXYKFKT03), the Provincial-level project of Hainan Province, Hainan Academy of Marine and Fishery Sciences (KYL-2023-01, KYL-2024-06), the Major Science and Technology Plan Project of Yazhou Bay Innovation Research Institute of Hainan Tropical Ocean University (2022CXYZD003), and the Hebei Provincial Natural Science Foundation of China (D2020409002).

Institutional Review Board Statement: Not applicable.

Informed Consent Statement: Not applicable.

Data Availability Statement: The data presented in this study are openly available in google earth engine at https://code.earthengine.google.com/362525640d920a99bfce22e869c5cb29.

Acknowledgments: The authors would like to thank the researchers who provided the open-source algorithms, which were extremely helpful to the research conducted in this paper. We also thank the anonymous reviewers and editors for their contributions.

Conflicts of Interest: The authors declare no conflicts of interest.

References

1. Liao, W.; Jiang, W. Evaluation of the spatiotemporal variations in the eco-environmental quality in China based on the remote sensing ecological index. *Remote Sens.* **2020**, *12*, 2462. [CrossRef]
2. Zhang, S.; Fan, W.; Li, Y.; Yi, Y. The influence of changes in land use and landscape patterns on soil erosion in a watershed. *Sci. Total Environ.* **2017**, *574*, 34–45. [CrossRef]
3. Xiaoli, M.; He, L.; Chong, H.; Qingsheng, L.I.U.; Gaohuan, L.I.U. Application progress of Google Earth Engine in land use and land cover remote sensing information extraction. *Remote Sens. Land Resour.* **2021**, *33*, 1–10.
4. Fu, D.; Xiao, H.; Su, F.Z.; Zhou, C.; Dong, J.; Zeng, Y.; Yan, K.; Li, S.W.; Wu, J.; Wu, W.Z.; et al. Remote sensing cloud computing platform development and Earth science application. *Natl. Remote Sens. Bull.* **2021**, *25*, 220–230. [CrossRef]
5. Campos-Taberner, M.; Moreno-Martínez, Á.; García-Haro, F.J.; Camps-Valls, G.; Robinson, N.P.; Kattge, J.; Running, S.W. Global estimation of biophysical variables from Google Earth Engine platform. *Remote Sens.* **2018**, *10*, 1167. [CrossRef]
6. Workie, T.G.; Debella, H.J. Climate change and its effects on vegetation phenology across ecoregions of Ethiopia. *Glob. Ecol. Conserv.* **2018**, *13*, e00366. [CrossRef]
7. Liu, C.; Li, W.; Wang, W.; Zhou, H.; Liang, T.; Hou, F.; Xu, J.; Xue, P. Quantitative spatial analysis of vegetation dynamics and potential driving factors in a typical alpine region on the northeastern Tibetan Plateau using the Google Earth Engine. *Catena* **2021**, *206*, 105500. [CrossRef]
8. Yuchuan, H.; Junnan, X.; Ahemaitihali, A.; Weiming, C.; Chongchong, Y.; Wen, H.; Zhiwei, Y.; Jie, T. Spatiotemporal Pattern and Driving Force Analysis of Vegetation Variation in Altay Prefecture based on Google Earth Engine. *J. Resour. Ecol.* **2021**, *12*, 729–742. [CrossRef]
9. Teluguntla, P.; Thenkabail, P.S.; Oliphant, A.; Xiong, J.; Gumma, M.K.; Congalton, R.G.; Yadav, K.; Huete, A. A 30-m landsat-derived cropland extent product of Australia and China using random forest machine learning algorithm on Google Earth Engine cloud computing platform. *ISPRS J. Photogramm. Remote Sens.* **2018**, *144*, 325–340. [CrossRef]
10. Galodha, A.; Gupta, S.K. Land surface temperature as an indicator of urban heat island effect: A google earth engine based Web-App. *Int. Arch. Photogramm. Remote Sens. Spat. Inf. Sci.* **2021**, *44*, 57–62. [CrossRef]
11. Oliphant, A.J.; Thenkabail, P.S.; Teluguntla, P.; Xiong, J.; Gumma, M.K.; Congalton, R.G.; Yadav, K. Mapping cropland extent of Southeast and Northeast Asia using multi-year time-series Landsat 30-m data using a random forest classifier on the Google Earth Engine Cloud. *Int. J. Appl. Earth Obs. Geoinf.* **2019**, *81*, 110–124. [CrossRef]
12. Ning, X.G.; Chang, W.T.; Wang, H.; Zhang, H.C.; Zhu, Q.D. Extraction of marsh wetland in Heilongjiang Basin based on GEE and multi-source remote sensing data. *Natl. Remote Sens. Bull.* **2022**, *26*, 386–396. [CrossRef]
13. Zurqani, H.A.; Post, C.J.; Mikhailova, E.A.; Schlautman, M.A.; Sharp, J.L. Geospatial analysis of land use change in the Savannah River Basin using Google Earth Engine. *Int. J. Appl. Earth Obs. Geoinf.* **2018**, *69*, 175–185. [CrossRef]
14. Fu, F.; Deng, S.; Wu, D.; Liu, W.; Bai, Z. Research on the spatiotemporal evolution of land use landscape pattern in a county area based on CA-Markov model. *Sustain. Cities Soc.* **2022**, *80*, 103760. [CrossRef]

15. Du, W.; Wang, Y.; Qian, D.; Lyu, X. Process and Eco-Environment Impact of Land Use Function Transition under the Perspective of "Production-Living-Ecological" Spaces—Case of Haikou City, China. *Int. J. Environ. Res. Public Health* **2022**, *19*, 16902. [CrossRef]
16. Cao, L.H.; Lang, Q.; Lei, K.; Wang, D.; Yang, K.; Yang, W. Analysis on landscape pattern dynamics and driving force in Yongding River Basin from 1980 to 2020. *J. Environ. Eng. Technol.* **2023**, *13*, 143–153.
17. Moenardy, D.F. Hainan province as the new free trade port. *Turk. J. Comput. Math. Educ. (TURCOMAT)* **2021**, *12*, 487–494.
18. Lin, X.; Fu, H. Spatial-Temporal Evolution and Driving Forces of Cultivated Land based on the PLUS Model: A Case Study of Haikou City, 1980–2020. *Sustainability* **2022**, *14*, 14284. [CrossRef]
19. Mohite, J.D.; Sawant, S.A.; Rana, S.; Pappula, S. Wheat area mapping and phenology detection using synthetic aperture radar and multi multi-spectral remote sensing observations. *Int. Arch. Photogramm. Remote Sens. Spat. Inf. Sci.* **2019**, *42*, 123–127. [CrossRef]
20. *GB 21010-2017*; Current land use classification. China National Standardization Administration: Beijing, China, 2017.
21. Wong, M.M.F.; Fung, J.C.H.; Yeung, P.P.S. High-resolution calculation of the urban vegetation fraction in the Pearl River Delta from the Sentinel-2 NDVI for urban climate model parameterization. *Geosci. Lett.* **2019**, *6*, 1–10. [CrossRef]
22. Descals, A.; Verger, A.; Yin, G.; Peñuelas, J. Improved estimates of arctic land surface phenology using Sentinel-2 time series. *Remote Sens.* **2020**, *12*, 3738. [CrossRef]
23. Dai, X.Q.; Shen, R.Q.; Wang, J.; Wang, J.; Zhou, J. Change Detection of Land Use in Henan Province Based on GEE Remote Sensing Cloud Platform. *J. Geomat. Sci. Technol.* **2021**, *38*, 287–294.
24. Fang, X.; Ying, Z.; Liang, Z.; Jia, L.I.U.; Xianghui, G.U. Extraction method of intertidal mangrove by using Sentinel-2 images. *Bull. Surv. Mapp.* **2020**, *2*, 49.
25. Rodriguez-Galiano, V.F.; Ghimire, B.; Rogan, J.; Chica-Olmo, M.; Rigol-Sanchez, J.P. An assessment of the effectiveness of a random forest classifier for land-cover classification. *ISPRS J. Photogramm. Remote Sens.* **2012**, *67*, 93–104. [CrossRef]
26. Olofsson, P.; Foody, G.M.; Herold, M.; Stehman, S.V.; Woodcock, C.E.; Wulder, M.A. Good practices for estimating area and assessing accuracy of land change. *Remote Sens. Environ.* **2014**, *148*, 42–57. [CrossRef]
27. Rong, T.; Zhang, P.; Jing, W.; Zhang, Y.; Li, Y.; Yang, D.; Yang, J.; Chang, H.; Ge, L. Carbon dioxide emissions and their driving forces of land use change based on Economic Contributive Coefficient (ECC) and Ecological Support Coefficient (ESC) in the lower Yellow river region (1995–2018). *Energies* **2020**, *13*, 2600. [CrossRef]
28. Li, Y.; Liu, G.; Huang, C. Dynamic changes analysis and hotspots detection of land use in the central core functional area of Jing-Jin-Ji from 2000 to 2015 based on remote sensing data. *Math. Probl. Eng.* **2017**, *2017*, 2183585. [CrossRef]
29. Wang, X.; Cheng, S.; Li, Y.; Cao, P.; Xiao, L. Study on land use change and ecological sensitivity in 30 years based on Landsat TM and OLI data—A case study of Qinling Mountains of Huyi District in Xi'an. *Quat. Sci.* **2022**, *42*, 1655–1672.
30. Zhuang, D.F.; Liu, J.Y. Study on the model of regional differentiation of land use degree in China. *J. Nat. Resour.* **1997**, *12*, 105–111.
31. Liu, F.; Yang, G.; Han, X.; Jia, G.; Wang, N. Spatial-temporal Evolution of Land Use and Spatial Autocorrelation Analysis in Horqin Sandy Land —A Case Study of Naiman Banner. *J. Northwest For. Univ.* **2020**, *35*, 148–157.
32. Wu, C.X.; Feng, Y.Z.; Zhao, H.; Bao, Q.; Lei, Y.Q.; Feng, J. Study on ecosystem service value of the Yellow River Basin in Gansu Province based on land use change. *J. Desert Res.* **2022**, *42*, 304–316.
33. Zhang, L.; Wu, Y.; Li, J.; Li, C. Analysis of land use and landscape pattern change in Myanmar section of the Golden Quadrangle Region in the border of China, Myanmar, Thailand and Laos. *World Reg. Stud.* **2018**, *27*, 21–33.
34. Li, Q.; Zhang, Z.; Wan, L.; Yang, C.; Zhang, J.; Ye, C.; Chen, Y. Landscape pattern optimization in Ningjiang River Basin based on landscape ecological risk assessment. *Acta Geogr. Sin.* **2019**, *74*, 1420–1437.
35. Xue, P.F.; Li, W.L.; Zhu, G.F.; Zhou, H.K.; Liu, C.L.; Yan, H.P. Changes in the pattern of an alpine wetland landscape in Maqu County in the first meander of the Yellow River. *Chin. J. Plant Ecol.* **2021**, *45*, 467. [CrossRef]
36. Deng, J.S.; Wang, K.; Hong, Y.; Qi, J.G. Spatio-temporal dynamics and evolution of land use change and landscape pattern in response to rapid urbanization. *Landsc. Urban Plan.* **2009**, *92*, 187–198. [CrossRef]
37. Yang, Y. Evolution of habitat quality and association with land-use changes in mountainous areas: A case study of the Taihang Mountains in Hebei Province, China. *Ecol. Indic.* **2021**, *129*, 107967. [CrossRef]
38. Crist, E.P.; Laurin, R.; Cicone, R.C. Vegetation and soils information contained in transformed Thematic Mapper data. In *Proceedings of the IGARSS'86 Symposium*; European Space Agency Publications Division: Paris, France, 1986; pp. 1465–1470.
39. Nedkov, R. Orthogonal transformation of segmented images from the satellite Sentinel-2. *C. R. L'academie Bulg. Sci.* **2017**, *70*, 687–692.
40. Wu, Q.; Miao, Y.; Chen, Q.; Hou, E.; Li, J. Monitoring on ecological environment in desertification mining areas based on Sentinel-2. *J. Min. Strat. Control Eng.* **2022**, *4*, 017017.